

# Kernel-phases for high-contrast detection beyond the resolution limit

Frantz Martinache<sup>a</sup>

<sup>a</sup>Subaru Telescope, 650 N. A'ohoku Place, HI 96720, USA

## ABSTRACT

The detection of high contrast companions at small angular separation appears feasible in conventional direct images using the self-calibration properties of interferometric observable quantities. In the high-Strehl regime, available from space borne observatories and using AO in the mid-infrared, quantities comparable to the closure-phase that are used with great success in non-redundant masking inteferometry, can be extracted from direct images, even taken with a redundant aperture. These new phase-noise immune observable quantities, called Kernel-phases, are determined a-priori from the knowledge of the geometry of the pupil only. Re-analysis of HST/NICMOS archive and other ground based AO images, using this new Kernel-phase algorithm, demonstrates the power of the method, and its ability to detect companions at the resolution limit and beyond.

## 1. INTRODUCTION

Imaging in the high angular resolution regime comes down to solving the problem of deconvolving an unknown object function from an ever changing point spread function (PSF). The development of adaptive optics (AO), now ubiquitous on major ground based observatories, dramatically changed this arena, by turning seeing limited images into diffraction limited ones.

High contrast detection is however currently limited by residual aberrations, responsible for the presence of speckles in the image. Different schemes have been developed to sort out the PSF from the object function in images, and a very successful approach is to use some form of diversity in the PSF: angular differential imaging<sup>1</sup> for instance, uses field-rotation to differentiate true companions from static speckles. Aggressive alternatives are becoming available with updated AO systems, often refered to as extreme-AO systems, with active optics that can be used to introduce phase diversities, for instance creating speckle free regions in the image<sup>2</sup> or estimating the coherence of speckles.<sup>3</sup>

This paper presents an alternative approach, based on an interferometric point of view of image formation. The approach builds on the recent development of non-redundant aperture masking interferometry.<sup>4,5</sup> The technique, first used in 1873 by Stephan in an attempt to measure the angular diameter of stars with the 80-cm baseline of the telescope of the Observatoire de Marseille, was revived by speckle interferometry,<sup>6</sup> the availability of large telescopes,<sup>7</sup> and the generalization of AO.<sup>8</sup>

Non-redundant masking interferometry takes advantage of the self-calibrating properties of an observable quantity called closure-phase.<sup>9</sup> This remarkable quantity exhibits a compelling property: it rejects all residual phase errors on the interferometer pupil. Moreover, because it is determined from the analysis of the final science detector, and not estimated from a separate “sensing” channel, it is immune to non-common path errors that are partly responsible for the presence of quasi-static speckles in regular images.

Once extracted, the closure phase can then be used as input of a parametric model, for instance of a binary star of variable characteristics (angular separation, position angle and luminosity contrast), to confirm or infirm the presence of a companion around a given source, while uncertainties provide contrast detection limits. This approach was for instance successfully used several references,<sup>10-14</sup> that typically report sensitivity of 5-6 magnitudes in the near-infrared at angular separations ranging from 0.5 to 4  $\lambda/D$ .

It was demonstrated that the notion of closure phase, requiring a strictly non-redundant aperture can be generalized to arbitrarily shaped (i.e. including redundant) pupils, if the wavefront quality is sufficient.<sup>15</sup> This

---

email: frantz@naoj.org

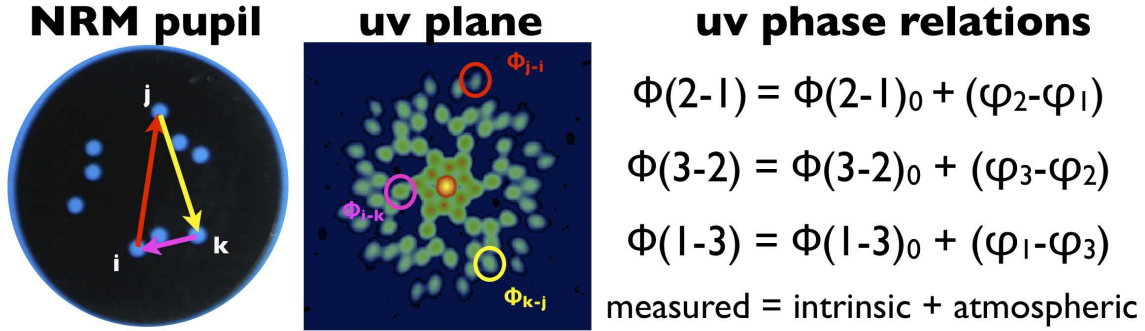


Figure 1. Example of closure phase relation. Superimposed on the image of the non-redundant pupil geometry shown in the left panel, is one of the possible closure triangles along which a closure relation can be formed. The central panel shows the powerspectrum of one image acquired with one such pupil: it is made of distinct regions, often referred to as splodges, each of which is associated to a baseline in the pupil. The three splodges associated to the baselines chosen in the left panel are highlighted. On the right, are written relations for the phases of each splodge: the measured phase is the sum of a term intrinsic to the target being observed (the “true” phase), and an atmospheric term: the piston along the baseline. The reader will quickly observe that by adding these three relations together, the atmospheric term simply vanishes, leading to a new observable quantity, called the closure-phase.

generalization of the closure-phase is coined Kernel-phase, since these closure relations form a basis for the null-space (or Kernel) of a linear operator. This paper first introduces the idea of generalized closure-phases, formulating the problem in terms of linear algebra. This new formulation is then used to show that it is not restricted to non-redundant apertures, if the wavefront quality is sufficient. Finally, the paper reports on a successful application of the Kernel-phase approach to a set of ground-based data, opening the doors of the super-resolution regime to a large number of observing programs.

## 2. GENERALIZED CLOSURE-PHASE

To understand how to generalize the idea of closure phase, it is useful to go back to the non-redundant masking (NRM) scenario and reformulate the problem in new terms. Fig. 1 shows how the problem is traditionally presented. A triangle of baselines in a non-redundant pupil is highlighted along with a typical powerspectra. Expressions for the three phase terms measured in the uv plane are listed. By adding the three measured phases, the piston terms cancel out: the resulting quantity, called a closure-phase, contains information about the observed source only, robust to piston and wavefront errors, making it extremely interesting.

The 9-hole NRM pupil presented in Fig. 1 allows to measure 36 distinct phases in the uv plane. These 36 relations can be written together in a matrix form:

$$\Phi = \Phi_0 + \mathbf{A} \cdot \varphi, \quad (1)$$

where  $\Phi$  is a 36-component vector coding the uv plane phases,  $\Phi_0$  a vector of same size, coding the true phases of the observed target,  $\varphi$  a 8-component vector representing the phase in the pupil (one aperture is chosen as a reference), and  $\mathbf{A}$  is a  $36 \times 8$  transfer matrix, whose properties form the core of this discussion.

For this example, each row of  $\mathbf{A}$  is essentially filled with zeros, except for two positions corresponding to the apertures making the baseline, that respectively contain +1 and -1. In general, a closure relation is a linear combination of rows of  $\mathbf{A}$  that give the zero vector. The closure-phase is a special case of one such linear relation, that simply adds together the appropriate series of three rows to give the zero vector. More complex relations involving more than three rows of  $\mathbf{A}$  can however be produced.

The total number of independent relations however remains constant, and is exactly 28 \* in this scenario. Using some algebra jargon is not inappropriate here: these closure relations form a basis for the left-hand null space (or Kernel) of  $\mathbf{A}$ . These relations can be summarized by a left hand operator  $\mathbf{K}$  that acts on  $\mathbf{A}$ , so that:

\* $(N - 1) \times (N - 2)/2$ , where  $N$  is the number of sub-apertures in the pupil in this NRM case

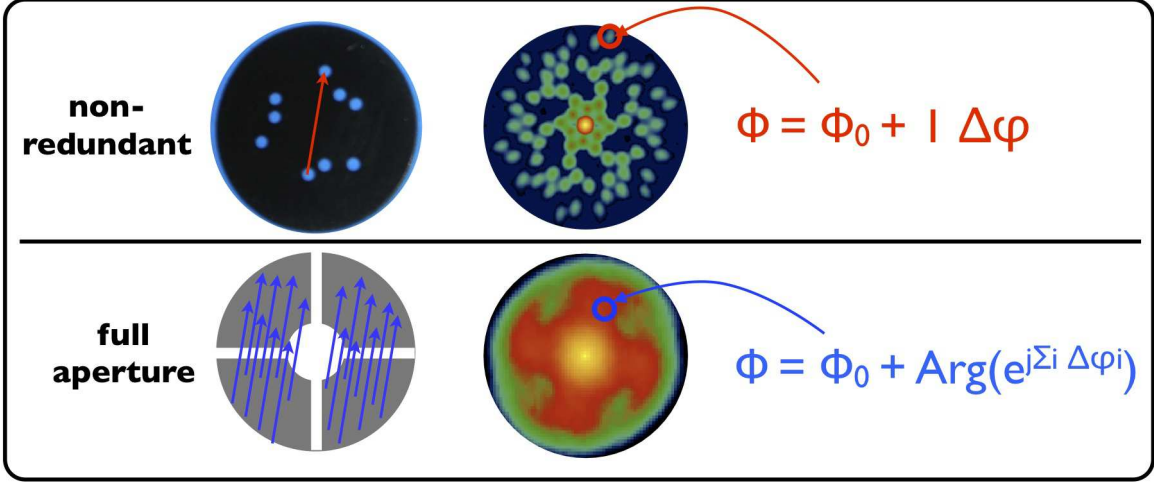


Figure 2. Comparison of the uv-plane phase measured with a NRM mask and with a conventional telescope aperture. In the latter scenario, a given baseline is sampled a large number of times within the pupil. The resulting expression for the phase is much more complex than in the non-redundant case: solving the deconvolution problem mentioned in the introduction, would mean being able to separate  $\Phi_0$  from a sum of random phasors. While this problem is indeed degenerate, AO makes it possible to extract closure-phase like quantities that do not depend on wavefront residuals (see text).

$$\mathbf{K} \cdot \mathbf{A} = \mathbf{0}. \quad (2)$$

Closure phase is convenient and easy to grasp. Moreover, it is a natural choice and the only possible closure relation when the pupil is made of only three sub-apertures. In practice for a baseline-rich pupil like the 9-hole case used as an example, closure-phase alone is not the best solution, as similar triangles in the pupil do exhibit correlated closure-phases. In addition to the closure phases, for NRM-interferometry data reduction, it is also customary to carry a correlation matrix, that is used during the modeling stage to produce reliable constraints on the parameters of the fit. Using this idea of generalized closure-phase, it is possible to find directly the relations that produce decorrelated observables. The next section will show how to do this for an arbitrary pupil shape.

### 3. KERNEL-PHASE

For arbitrarily shaped pupils (see the comparison NRM vs full aperture in Fig. 2), there is an extra complication, as the useful interferometric signal  $\Phi_0$  finds itself buried under multiple phase error contributions, which results into a fairly complex (non-linear) expression for the uv-phase:

$$\Phi^k = \Phi_0^k + \text{Arg}(e^{j\sum_i \Delta\varphi_i}), \quad (3)$$

where  $i$  is an index to keep track of the  $r$  identical baselines in the pupil, contributing to the same region of the uv plane. With a good wavefront correction (this approach has been validated both on space-based and ground-based data) - eq. 3 can be linearized as follows:

$$\Phi^k = \Phi_0^k + (1/r)\sum_i \Delta\varphi_i, \quad (4)$$

and the entire problem can again be written in the matrix form of eq. 1, with a modified transfer matrix. In order to maintain some resemblance with the previous case, it has been preferred so far to split this transfer matrix into a product of two matrices: a diagonal matrix  $1/\mathbf{R}$  that encodes the redundance of the baselines, and  $\mathbf{A}$ . In the (redundant) full aperture case, each row of  $\mathbf{A}$  now contains more than just two non-zero values, that are however still either  $-1$  or  $1$ . The problem is now written as follows:

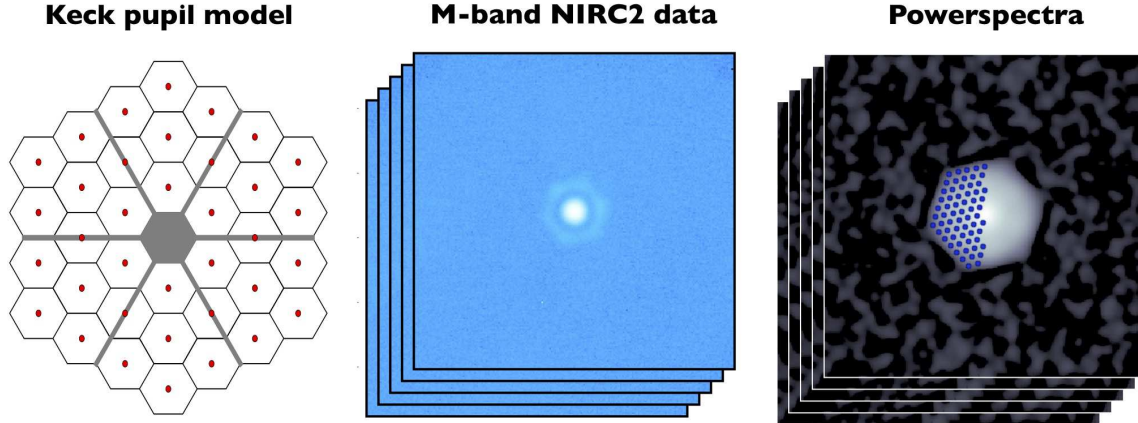


Figure 3. Left panel: Model of the Keck II Telescope pupil used for the determination of Kernel-phase relations. Each of the 36 segments of the pupil is reduced to a single point. Middle panel: example of M-band frame acquired with NIRC2. Right panel: each frame is Fourier-transformed, and this panel shows the powerspectrum (square modulus of the complex function), in non-linear scale. The uv sample points matching the model of the pupil are overlaid. For these locations of the uv-plane, the phase is extracted and combined into Kernel-phases using the relations introduced in Section 3.

$$\mathbf{R} \cdot \Phi = \mathbf{A} \cdot \varphi + \mathbf{R} \cdot \Phi_0. \quad (5)$$

Even with this new problem, it is possible to find a left hand operator  $\mathbf{K}$  that verifies eq. 2. While it is possible to find by hand friendly closure-phase like relations if the pupil geometry is not too complex, it quickly becomes difficult as the matrix  $\mathbf{A}$  can get quite big. A very efficient way to achieve this goal is to calculate the singular value decomposition (SVD) of  $\mathbf{A}^T$ . If the phase in the pupil can be accurately described by a vector of size  $N - 1$ , that produces  $M$  distinct uv points (some of which are highly redundant), the SVD algorithm<sup>16</sup> allows to decompose the  $(N - 1) \times M$  matrix  $\mathbf{A}^T$  as the product of a  $(N - 1) \times M$  column-orthogonal matrix  $\mathbf{U}$ , an  $M \times M$  diagonal matrix  $\mathbf{W}$  with positive or zero elements (the so-called singular values), and the transpose of an  $M \times M$  orthogonal matrix  $\mathbf{V}$ :

$$\mathbf{A}^T = \mathbf{U} \cdot \mathbf{W} \cdot \mathbf{V}^T. \quad (6)$$

Among other properties, the SVD explicitly constructs an orthonormal basis for the null-space of a matrix: with the notations used in this paper, the columns of  $\mathbf{V}$  that correspond to singular values equal to zero are exactly what needs to fill in the rows of  $\mathbf{K}$ . These relations, conveniently orthogonal, when applied to Eq. 5 produce observable quantities that just like closure phase, are independent from instrumental and atmospheric phase. These observable quantities are called Kernel-phases, since they relate to the Kernel of the transfer matrix  $\mathbf{A}$ . The following Section will present results of application of this method.

#### 4. FIRST GROUND-BASED RESULTS USING KERNEL-PHASE

The Kernel-phase approach was successfully applied to two series of narrow-band images acquired with the Near Infrared Camera and Multiobject Spectrometer (NICMOS) onboard the Hubble Space Telescope.<sup>15</sup> In one case, a positive detection of a known 10 : 1 binary companion (GJ 164 B) with milli-arcsecond astrometric prediction, at angular separation  $0.6 \lambda/D$  was made. In the other case, supposed to be a single calibration star (SAO 179809), a series of Monte Carlo simulations demonstrated that at angular separation  $0.5 \lambda/D$  (i.e. 80 mas at  $\lambda = 1.9 \mu\text{m}$ ), a contrast limit better than 50 : 1 is possible at the 99 % confidence level. At angular separation  $1 \lambda/D$ , this limit increases to 200 : 1 at the same confidence level. For this paper, the technique was applied to a series of M-band images acquired with NIRC2 on the Keck II telescope of the W.M. Keck Observatory.

Application of the Kernel-phase technique starts with building a model of the pupil of the telescope. The left panel of Fig. 3 shows the model used for this data analysis: the segmented aperture of the Keck II Telescope

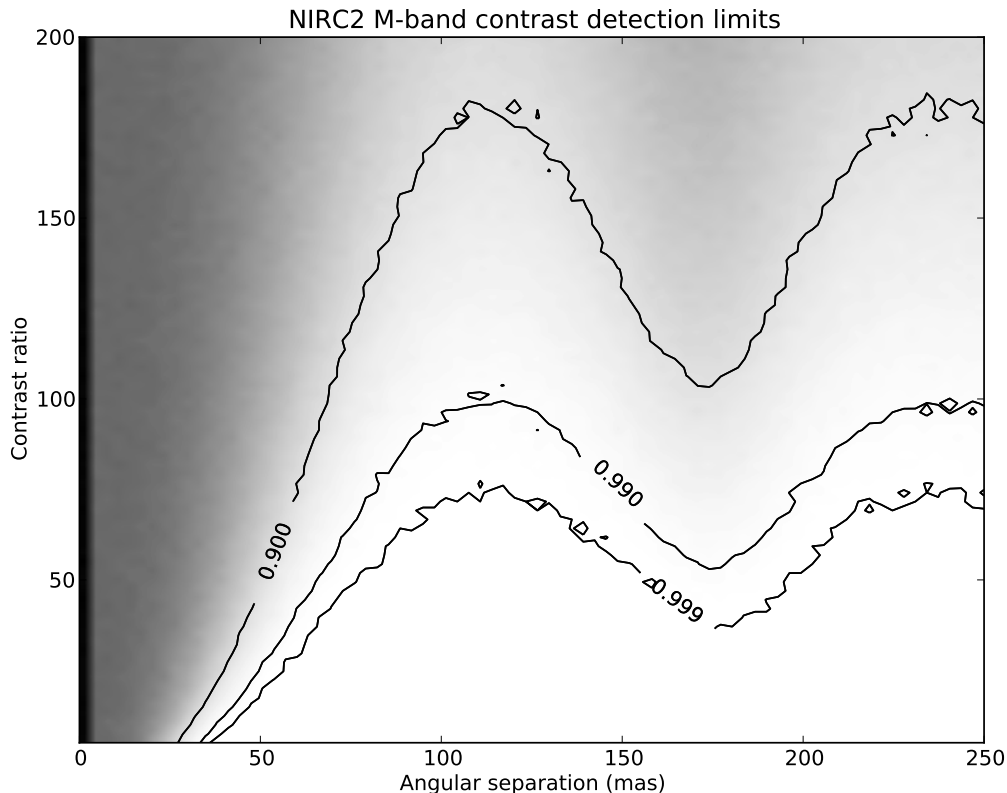


Figure 4. Levels of confidence in the detection of a companion in the (angular separation - contrast) space, using the proposed Kernel-phase algorithm on M-band data acquired at the Keck II Telescope, using NIRC2. A darker color indicates a region of lower confidence level. Three levels are highlighted: the 90 %, 99 % and 99.9 % confidence levels. At angular separation  $0.5 \lambda/D$ , a 20:1 contrast detection appears feasible at the 99.9 % confidence level. Note that the highlighted contours closely match the radial evolution of the diffraction pattern by the Keck II pupil.

is reduced to a series of 36 points. The pupil phase  $\varphi$  is therefore assembled into a 35-component vector. This 35-component pupil phase vector maps in the  $uv$  plane onto a hexagonal grid of 63 distinct points, shown in the right panel of Fig. 3. The transfer matrix  $\mathbf{A}$  is therefore a  $35 \times 63$  rectangular matrix. The SVD reveals that 18 singular values are non-zero, leaving  $63 - 18 = 45$  Kernel-phase relations.

Once the  $uv$ -points chosen and the matching Kernel-phase relations identified, they can be saved in a template and used after extraction of the phase from the data. The data used in this example consist of one target and two calibrators<sup>†</sup>. For each source, there is an average of 20 frames. After dark subtraction, and flat-fielding, each frame is simply Fourier transformed. The left hand side of the equation 5 (i.e.  $\mathbf{R} \cdot \Phi$ ) can be acquired by reading directly the imaginary part of the complex visibility (the Fourier transform), at the pre-defined  $uv$ -plane locations. The uncertainty associated with the measurement of each sample is estimated from the dispersion of the signal in the direct neighborhood of the  $uv$ -plane sample points.

Kernel-phases are constructed using the pre-determined relations for each frame, then averaged per source, and uncertainties are propagated. The final retained series of 45 Kernel-phases is the weighted average for all frames. Just like for closure-phase, calibration of Kernel-phase is simply a matter of subtracting the Kernel-phase of one or more calibrators from the ones recorded on the source of interest.

<sup>†</sup>data courtesy of Adam Kraus and Michael Ireland

While, no obvious detection can be reported from this data analysis, the final calibrated closure phases were used as input in a Monte Carlo simulation to determine contrast detection limits.

The sampling in the uv-plane (cf. Fig. 3) is sufficiently uniform for the sensitivity to be only a very weak function of the position angle of a potential companion. Sensitivity is however expected to be a strong function of angular separation: it is not difficult to believe that the detection of a companion will be easier if it is located between two diffraction rings than if it lands exactly on a ring. Note that the sampling also limits the outer working angle of the analysis to  $\sim 4\lambda/D$ , beyond which direct analysis of the image is expected to provide superior results anyway.

Fig. 4 summarizes the detection limits with this data-set. The overall structure of this sensitivity 2D plot is strikingly similar to what was reported after a comparable analysis of NICMOS data.<sup>15</sup> The three highlighted confidence levels closely match the radial evolution of the Airy pattern for Keck II. At  $0.5 \lambda/D$ , a 20:1 contrast detection appears feasible with a high (99.9 %) confidence level. At  $1 \lambda/D$ , this limit rises to 70:1.

While quite encouraging, it is not clear yet what is constraining the detection limits on this dataset. In the near future, a comprehensive set of simulations including background, readout and photon noise in addition to wavefront errors will help define observing strategies that will maximize the Kernel-phase’s potential for high contrast detections at the diffraction limit and in the super-resolution regime.

## 5. CONCLUSION

Closure-phase was shown to be a special case of a wider family of observable quantities immune to phase noise and non-common path errors. While invented for, and perfectly adapted to interferometers with a limited number of apertures (with a minimum of three, that is), closure-phase is not necessarily the most appropriate of these observable quantities when dealing with baseline-rich apertures of modern NRM-interferometry. Using a very general linear algebraic approach, it was shown that the notion of closure-phase can be generalized, and this generalization extends the applicability of the technique to conventional full-aperture images, if wavefront quality is sufficient.

Completing already published work that demonstrated potential of the method on archive narrow-band HST/NICMOS data, and achieved moderate contrast detection in the super resolution regime with good astrometric precision, this paper showed that Kernel-phases can now be extracted from ground based broad-band high-Strehl AO data, opening the doors of the super-resolution regime that has so far been the exclusivity of NRM-interferometry, even with a highly redundant pupil.

In addition to the already available HST/NICMOS archive data awaiting re-analysis with the potential to lead to new detections in the super-resolution regime and/or to improved detection limits, there are multiple types of ground-based AO observing programs, mostly in L- and M-band where the AO correction is at its best, that can now also take advantage of this technique.

## ACKNOWLEDGMENTS

The author thanks Adam Kraus and Michael Ireland for sharing the NIRC2 data-set used for this demonstration of the technique done in this paper. This work was supported in part by the Jet Propulsion Laboratory uncr contract 1379504.

## REFERENCES

- [1] Marois, C., Lafrenière, D., Doyon, R., Macintosh, B., and Nadeau, D., “Angular Differential Imaging: A Powerful High-Contrast Imaging Technique,” *ApJ* **641**, 556–564 (Apr. 2006).
- [2] Malbet, F., Yu, J. W., and Shao, M., “High-Dynamic-Range Imaging Using a Deformable Mirror for Space Coronagraphy,” *PASP* **107**, 386–+ (Apr. 1995).
- [3] Guyon, O., Pluzhnik, E., Martinache, F., Totems, J., Tanaka, S., Matsuo, T., Blain, C., and Belikov, R., “High-Contrast Imaging and Wavefront Control with a PIAA Coronagraph: Laboratory System Validation,” *PASP* **122**, 71–84 (Jan. 2010).

- [4] Readhead, A. C. S., Nakajima, T. S., Pearson, T. J., Neugebauer, G., Oke, J. B., and Sargent, W. L. W., “Diffraction-limited imaging with ground-based optical telescopes,” *AJ* **95**, 1278–1296 (Apr. 1988).
- [5] Nakajima, T., Kulkarni, S. R., Gorham, P. W., Ghez, A. M., Neugebauer, G., Oke, J. B., Prince, T. A., and Readhead, A. C. S., “Diffraction-limited imaging. II - Optical aperture-synthesis imaging of two binary stars,” *AJ* **97**, 1510–1521 (May 1989).
- [6] Labeyrie, A., “Attainment of Diffraction Limited Resolution in Large Telescopes by Fourier Analysing Speckle Patterns in Star Images,” *A&A* **6**, 85–+ (May 1970).
- [7] Tuthill, P. G., Monnier, J. D., Danchi, W. C., Wishnow, E. H., and Haniff, C. A., “Michelson Interferometry with the Keck I Telescope,” *PASP* **112**, 555–565 (Apr. 2000).
- [8] Tuthill, P., Lloyd, J., Ireland, M., Martinache, F., Monnier, J., Woodruff, H., ten Brummelaar, T., Turner, N., and Townes, C., “Sparse-aperture adaptive optics,” in [*Advances in Adaptive Optics II. Edited by Ellerbroek, Brent L.; Bonaccini Calia, Domenico. Proceedings of the SPIE, Volume 6272, pp. (2006).*], (July 2006).
- [9] Jennison, R. C., “A phase sensitive interferometer technique for the measurement of the Fourier transforms of spatial brightness distributions of small angular extent,” *MNRAS* **118**, 276–+ (1958).
- [10] Lloyd, J. P., Martinache, F., Ireland, M. J., Monnier, J. D., Pravdo, S. H., Shaklan, S. B., and Tuthill, P. G., “Direct Detection of the Brown Dwarf GJ 802B with Adaptive Optics Masking Interferometry,” *ApJ* **650**, L131–L134 (Oct. 2006).
- [11] Martinache, F., Lloyd, J. P., Ireland, M. J., Yamada, R. S., and Tuthill, P. G., “Precision Masses of the Low-Mass Binary System GJ 623,” *ApJ* **661**, 496–501 (May 2007).
- [12] Ireland, M. J., Kraus, A., Martinache, F., Lloyd, J. P., and Tuthill, P. G., “Dynamical Mass of GJ 802B: A Brown Dwarf in a Triple System,” *ApJ* **678**, 463–471 (May 2008).
- [13] Kraus, A. L., Ireland, M. J., Martinache, F., and Lloyd, J. P., “Mapping the Shores of the Brown Dwarf Desert. I. Upper Scorpius,” *ApJ* **679**, 762–782 (May 2008).
- [14] Martinache, F., Rojas-Ayala, B., Ireland, M. J., Lloyd, J. P., and Tuthill, P. G., “Visual Orbit of the Low-Mass Binary GJ 164 AB,” *ApJ* **695**, 1183–1190 (Apr. 2009).
- [15] Martinache, F., “Kernel Phase in Fizeau Interferometry,” *ApJ* **724**, 464–469 (Nov. 2010).
- [16] Press, W. H., Teukolsky, S. A., Vetterling, W. T., and Flannery, B. P., [*Numerical recipes in C The Art of Scientific Computing, 2nd edition*] (2002).